

Red blood cell aggregate flux in a bifurcating microchannel

E. Kaliviotis<sup>\*1,2</sup>, D. Pasias<sup>1</sup>, J.M. Sherwood<sup>3</sup>, and S. Balabani<sup>2</sup>

<sup>1</sup>*Department of Mechanical Engineering and Materials Science and Engineering, Cyprus University of Technology, Cyprus*

<sup>2</sup>*Department of Mechanical Engineering, University College London, UK*

<sup>3</sup>*Department of Bioengineering, Imperial College London, UK*

*\*Corresponding author: E. Kaliviotis, tel.: 0035725002289, [e.kaliviotis@cut.ac.cy](mailto:e.kaliviotis@cut.ac.cy)*

---

## **Abstract**

Red blood cell aggregation plays a key role in microcirculatory flows, however, little is known about the transport characteristics of red blood cell aggregates in branching geometries. This work reports on the fluxes of red blood cell aggregates of various sizes in a T-shaped microchannel, aiming to clarify the effects of different flow conditions in the outlet branches of the channel. Image analysis techniques, were utilised, and moderately aggregating human red blood cell suspensions were tested in symmetric (~50-50%) and asymmetric flow splits through the two outlet (daughter) branches. The results revealed that the flux decreases with aggregate size in the inlet (parent) and daughter branches, mainly due to the fact that the number of larger structures is significantly smaller than that of smaller structures. However, when the flux in the daughter branches is examined relative to the aggregate size flux in the parent branch an increase with aggregate size is observed for a range of asymmetric flow splits. This increase is attributed to size distribution and local concentration changes in the daughter branches. The results show that the flow of larger aggregates is not suppressed downstream of a bifurcation, and that blood flow is maintained, for physiological levels of red blood cell aggregation.

**Keywords:** Blood flow, red blood cell aggregate flux, micro-PIV, image processing techniques

## **1. Introduction**

Microfluidic blood flows have received considerable attention in recent years due to the opportunities these systems offer for research on fundamental phenomena occurring at the microscale, and for the development of lab on chip and diagnostic systems. Studying blood flow at such scales allows key flow and structural characteristics of blood, arising from its multiphase nature, to be studied in great depth [1,2]. The complex characteristics of microscale blood flow are mainly due to the presence of red blood cells (RBCs) which constitute the majority of the cellular matter of blood. The red blood cell is a deformable corpuscle resembling a disk (~8 $\mu$ m diameter) with its centre compressed (thicknesses at the edge and centre are ~2.8 and ~1.4  $\mu$ m respectively) and accounts for ~45% of the volume of the fluid. The concentration of RBCs in the plasma, which is the continuous phase of the fluid, and their deformability play a part in rendering blood a non-Newtonian fluid; however, it is the tendency of RBCs to aggregate that mainly causes the distinctive increase of blood viscosity at low shear rates. Like most suspensions, blood exhibits a shear thinning behaviour, which is due to the reversible RBC aggregation phenomenon at low shear rates. RBC aggregation occurs mainly in the presence of the plasma protein fibrinogen [3] and is diminished by shear forces developed in the flow. The viscoelastic properties of blood have been examined in early [4-6] as well as more recent studies [7,8], illustrating the weakly-attractive suspension nature of blood. The fact that the flow characteristics may play a role on the aggregation of RBCs has been observed in the studies of Tomaiuolo et al. [9] and Claveria et al. [10], where RBC clustering in microconfined Poiseuille flow is observed independent of aggregative forces. The cluster length was observed to be pressure drop dependent and the formation of larger clusters was favoured by longer residence times in the shear conditions

tested [9]. In the study of Clavería et al. [10], red blood cell suspensions in physiological buffer solutions (PBS) and in Dextran solutions at different concentrations were used to mimic healthy and pathological levels of fibrinogen in capillary configurations. It was found that there is a strong increase in the number of isolated cells between the low and the high stress flow cases implying more intense aggregation in the low stress cases. In the same study it was found that at smaller velocities, the cells are mainly in the axial-centered parachute configuration, but at higher velocities RBCs are found in an off-centered position.

Our previous work on red blood cell transport in straight and bifurcating microchannels (Sherwood et al. [11-13] and Kaliviotis et al. [14,15]) has investigated the cell depleted layer (CDL) formed near the walls, the spatial variation of RBC concentrations, the phenomenon of plasma skimming and the aggregate size distribution. A comprehensive literature review on these characteristics for *in vivo* and *in vitro* studies was also provided therein.

The aggregate size distribution in the flow was examined by the authors for flow in a straight rectangular microchannel (250x50 microns width and height respectively) through bulk and local aggregation indices [14]. A local aggregation index,  $A^*$ , based on detecting the iso-intensity patterns formed by the aggregated cells was developed to characterise the aggregate size. This index allowed the quantification of the organisation of aggregates in the plane of shear and highlighted the combined effect of haematocrit and flow velocity on local aggregation characteristics. In the aforementioned study it was also shown that large RBC aggregates show a preference towards the central locations of the channel and this was explained in view of the lower shear forces developed in the regions, compared to those developed close to the boundaries of the flow configuration. The same methodology was recently applied to RBC flows in a T-type bifurcating microchannel [15] in order to examine the aggregate size characteristics. The experiments were performed with aggregating and non-aggregating samples and the effect of the daughter branch flow rate ratio (i.e. the ratio of daughter branch flow rate to this in the parent branch) on the aggregate size characteristics was examined. The results showed that the mean aggregate size decreases in the lower flow rate branches and this was attributed to two characteristics: a) the existence of regions near the channel walls in the parent branch, which are depleted by aggregates of certain sizes, and b) to the change in the exact flow split location in the outlet of the parent branch with the change in the flow ratio.

RBC aggregate size distributions have also been considered in the studies of Mehri et al. [1] and Yeom et al. [2]. Yeom et al., used a technique based on counting the number of RBCs per aggregate at low haematocrits (10%), in a very thin chamber (10  $\mu\text{m}$  height) while Mehri et al. quantified the distribution of RBC aggregates in a rectangular geometry (110x60 $\mu\text{m}$  width and height) and at low haematocrits (5, 10 and 15%) using image processing techniques. It was shown that the average aggregate size in the microchannel decreased with shear rate. For example, for a 15% haematocrit the aggregate size decreased from  $\sim 160\mu\text{m}^2$  to  $\sim 110\mu\text{m}^2$  for pseudo-shear rates of 2.5 and  $7.4\text{s}^{-1}$  respectively. In the  $2.5\text{s}^{-1}$  case, 41% of aggregates contained 6 or more RBCs, compared to only 16% for the  $7.4\text{s}^{-1}$  case.

The aforementioned studies used image analysis techniques for the characterisation of aggregate size, as they provide unequivocal data [16]. However, there are certain limitations in the use of image analysis for aggregate characterisation, with the main one been the RBC concentration, which affects the image quality due to high light absorption. Kaliviotis et al. [14] addressed these imitations by developing advanced image processing techniques, taking advantage of the specific features of RBC aggregation mentioned earlier.

A great number of additional techniques for aggregation characterisation at bulk levels exist in the literature, and commercial instruments are also available [17]. However, in microscale blood flows, and in particular in bifurcating geometries, where the flow and haematocrit conditions are not uniform, the local characteristics of aggregation play a major part in blood transport. For instance, it is still not clear if, and to what extent, RBC aggregation is

beneficiary or harmful for the circulation [18]. The flux of aggregates of different sizes in the vasculature could reveal information about the transport of the formed structures under aggregating conditions.

To the best of our knowledge, there are no studies in the literature quantifying RBC aggregate flux characteristics in bifurcating microchannel flows. In this paper, we report on a study of RBC aggregate size fluxes in a T-junction for the first time, estimated through analysis of the bifurcating flows reported in Sherwood et al. [11,12], using the aggregate detection methodology developed by Kaliviotis et al. [14,15]. The paper is structured as follows: in the *Methodology* section the technique for flux calculation is described and information regarding sample preparation, the flow system, and flux calculation is provided; in the *Results and discussion* section the presentation and analysis of the RBC aggregate size flux is presented for 34 different flow splits (i.e. 68 cases) together with an elaboration on the findings. The paper is closed with concluding remarks.

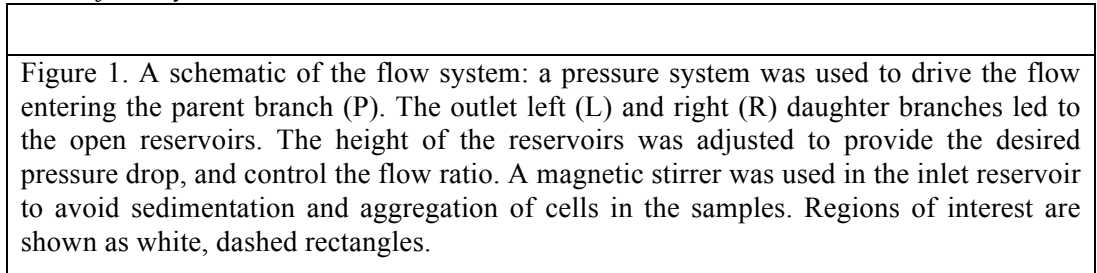
## 2. Methodology

Details for the experimental apparatus, sample preparation, flow measurement methodology and aggregate size characterization can be found elsewhere [11,12,14] and only a brief description is provided here.

### 2.1 Sample preparation

Samples were acquired with the approval of the Southeast London Ethics Committee (ref: 10/H0804/21). Blood was collected from healthy volunteers into vacuum tubes (BD) preloaded with 1.8 mg/ml EDTA. The RBCs were washed twice in Phosphate Buffered Saline (PBS), centrifuged at 3000 rpm, and suspended in PBS containing D2000 (5g/l). Dextrans are glucan polymers of various molecular weights that are widely used to induce aggregation between red blood cells. The aggregation dependency on Dextran concentration and molecular weight has been illustrated in various studies [19,20]. The haematocrit was adjusted to 25% by volume which is considered physiological for the microchannel dimensions used [21,22]. For consistency all experiments were conducted with a single sample.

### 2.2 The flow system



A microchannel (width  $W = 100\mu\text{m}$  and depth  $D = 40\mu\text{m}$ ) was fabricated from SU8 using photolithography (Epigem, Redcar, UK), and is shown in Figure 1. The sample was perfused through the parent branch of the microchannel by applying a pressure to the sealed inlet reservoir. The pressure in the inlet reservoir was controlled with a pressure control system comprising an actuated needle valve and a compressed nitrogen source. The fluid in the inlet reservoir was continuously mixed with a magnetic stir bar, in order to minimise the effects of RBC sedimentation. The stirrer was stopped when acquiring data.

The inlet reservoir pressure was set to a value resulting in a mean velocity of  $320\mu\text{m s}^{-1}$  in the parent branch. This velocity is physiological and comparable to the average cross-sectional velocities measured in the arterioles of the human conjunctiva (see for example the studies of Koutsiaris et al. [23,24]). The distribution of flow between the two daughter branches (flow split) was controlled by means of hydrostatic pressure difference by independently adjusting the height of the outlet reservoirs using micrometer stages. Between acquisitions, the channel

was initially perfused at a high flow rate in order to ensure uniform hematocrit throughout the channel and system; subsequently the pressure was reduced to the desired level and 20s were allowed for aggregation to reach a steady state before acquisition commenced [12].

### 2.3 Microscopy and microPIV system

An inverted microscope (Leica DM ILM, Germany) was used to visualise the flow, with the focal plane set to the centre of the channel. A halogen light-source was used for illumination and images were acquired using a CMOS camera (IDT X3, Tallahassee, USA) at 125Hz. Multi-pass ensemble averaged PIV processing was carried out on each of the data sets, providing a final window size of 8x8 pixels and a vector spacing of 4 pixels (2.6  $\mu\text{m}$ ) using JPIV software ([www.jpiv.vennemann-online.de](http://www.jpiv.vennemann-online.de)). The spatial resolution was 0.65  $\mu\text{m}/\text{pixel}$ . A normalised median test was utilised to identify the invalid vectors, which were replaced with the median of the surrounding vectors. For the estimation of the flow rate for each branch, spatially averaged velocity profiles were acquired in the regions indicated by the region of interest in Figure 1. The flow ratio was defined as the ratio between the flow rate in the daughter and the parent branch:  $Q^*=Q_D/Q_P$ , and was estimated from the average velocities ( $U$ ) using PIV, according to  $Q^*=U_D/U_P$ , as the cross-sectional area was the same in all branches. The velocity fields produced using the JPIV software were further processed in Matlab to derive the flux for each RBC aggregate size range examined. The velocity field in Figure 2 is derived from an aggregating case with  $Q^*\sim 0.13$ . The vector density and channel length is reduced for clarity of presentation.

Figure 2. The velocity field derived from an aggregating case with $Q^*\sim 0.13$ . The vector density and the length of channel are reduced for clarity of presentation.
---

### 2.4 RBC aggregate size characterisation

The RBC aggregate detection method was developed on the basis that connected RBCs (rouleaux) cause continuous iso-intensity patterns to appear in the captured images. These patterns can be identified with edge detection algorithms. It was shown that these iso-intensity areas increase almost linearly with the number of RBCs per aggregate for small aggregates of up to 15 RBCs per aggregate [14,15]. The detection algorithm is briefly described below.

The main image processing stages included image *pre-processing* to improve image quality, *identification of the local intensity gradients*, *blurring correction*, *edge detection*, *noise elimination*, and *statistical analysis* of the data.

The regions in which the local gradients were above a threshold value were defined as edge points. The gradient threshold value was defined by calibrating on a non-aggregating case and used blindly in the rest of the aggregation cases. This stage involved the identification of a threshold value that resulted in a mean edge area equal to a characteristic RBC area  $A_c$ .  $A_c$  was defined according to the fact that different configurations of one RBC could be seen in the images due to the rotation and deformation of the cells in the flow; the estimated edge size of one RBC when viewed from the flat side, was estimated at  $\sim 45\mu\text{m}^2$ , whereas the edge area of one RBC when seen laterally was  $\sim 10\mu\text{m}^2$ . A low value of  $A_c= 15\mu\text{m}^2$  was set based on the fact that there are various limitations imposed by the nature of the imaged data. These limitations affected the overall quality of the images and prevented complete RBC edges to be resolved. Pixels smaller than 50% of the characteristic RBC edge area were discarded as noise. The image processing technique was validated against other image processing and electrorheology techniques [25] and limitations have been discussed therein [14].

Figure 3 illustrates the performance of the technique for representative cases; magnified sections of images are provided in order to visually inspect the efficacy of the image processing algorithm. Figures 3(a) and 3(b) show the original and processed result for a non-aggregating case (left daughter branch, with  $Q^*=0.5$ ). Figures 3(c) to 3(h) show the original and resulting images for aggregating samples at various locations in the channel; 3(c) and

3(d): parent branch; 3(e) and 3(f): daughter branch,  $Q^*=0.36$ ; 3(g) and 3(h): daughter branch,  $Q^*\sim 0.28$ . Images 3(e) to 3(h) show that edges are detected for aggregates found in plasma background and for aggregates appearing within the bulk of the volume of the cells.

(a)	(b)	(c)	(d)
(e)	(f)	(g)	(h)
Figure 3. Representative processed images: (a) and (b) no aggregation; (c) to (h) aggregating samples at different locations in the channel. (a) and (b): daughter branch, with $Q^*\sim 0.5$ ; (c) and (d): parent branch, $Q^*\sim 0.46$ ; (e) and (f): daughter branch, $Q^*\sim 0.36$ ; (g) and (h): daughter branch, $Q^*\sim 0.28$ .			

### 2.4 Aggregate size flux calculation

The flux for each flow split was defined and calculated similarly to Guidi et al. [26], as the number of aggregates of certain size, per cross sectional area, per second. The existing data was obtained in the direction of flow for specific regions of interest, ROIs (see the schematic in Figure 1 for the ROIs in the channel). This means that the information is extracted from a specific volume in the flow configuration. Therefore, the flux was calculated using the velocity of the aggregates:

$$F_{A^*} = U N_{A^*} V^{-1}$$

where  $N_{A^*}$  is the number of aggregates of size  $A^*$ ,  $U$  the mean velocity of particles with size  $A^*$  (within a range of 10% of a specific value), and  $V$  the volume of the flow configuration in the ROI.  $A^*$  is the detected edge area of a single structure in an instantaneous image normalised by the characteristic area of one RBC,  $A_c$ . The velocity of the centroid of the aggregate structures was used in the flux calculation; the centroid coordinates of the aggregated structure were obtained by image processing of the data. Aggregate sizes  $A^*$  ranging from 1 to 7 were examined in the study. 34 different flow splits (e.g. 80-20, 70-30, 60-40, etc.) were considered resulting in 68 different flow ratios  $Q^*$  (ranging from 0.02 up to 0.48 for the right daughter, and from 0.55 up to 0.96 in the left daughter).

In order to examine how aggregates are transported in the daughter branches relative to the parent branch, a normalized flux quantity  $F^*$  (i.e.  $F^* = F_{\text{Daughter}} / F_{\text{Parent}}$ ) was introduced for each aggregate size  $A^*$  examined in the study (1 to 7) and plotted against the normalized flow ratio  $Q^*$ .

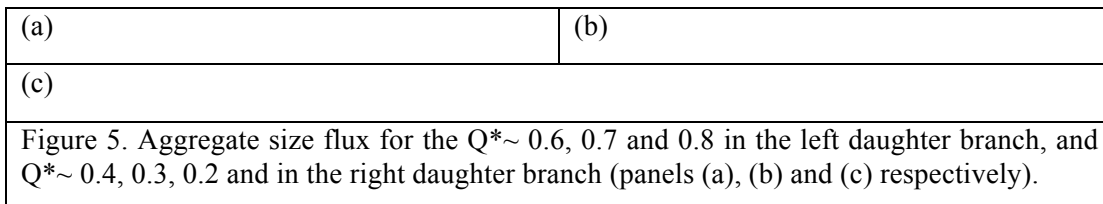
### 3. Results and discussion

Figure 4a shows the edge area distribution in the parent branch for a flow ratio  $Q^*$  of  $\sim 0.1$  as reported in Kaliviotis et al. [15]. The RBC aggregation phenomenon causes distinct changes in the microstructure of the fluid and this is reflected in the statistics of the data in Figure 4a (the distribution is left-truncated at 0.5 for the purpose of noise reduction). The mean aggregate size value is  $\sim 2$  within a population of approximately 70000 structures (from 400 images). The area  $A^*$  for one RBC edge is equal to unity according to the normalisation parameter  $A_c$ . Figure 4b shows the spatial distribution of aggregate size  $A^*$  in the channel for the extreme case of  $Q^*=0.02$  in the right daughter branch (positive  $x^*$  range). The figure illustrates that for low  $Q^*$  (below  $\sim 0.2$ ) the mean aggregate size decreases compared to the mean size in the opposite branch. This behaviour has been examined in Kaliviotis et al. [15] and has been explained on the basis of the existence of regions near the parent branch walls, which are depleted by aggregates of certain sizes. This depleted region, in combination with the fact that the flow split location in the outlet of the parent branch changes with flow ratio, affects the transportation of aggregates of certain sizes in the low flow ratio branches.

(a)	(b)
Figure 4. (a) Detected edge area $A^*$ distribution for $Q^* \sim 0.1$ and from 400 images ( $n\sim 70000$ ) as reported in Kaliviotis et al. [15]. (b) The location of the detected aggregate	

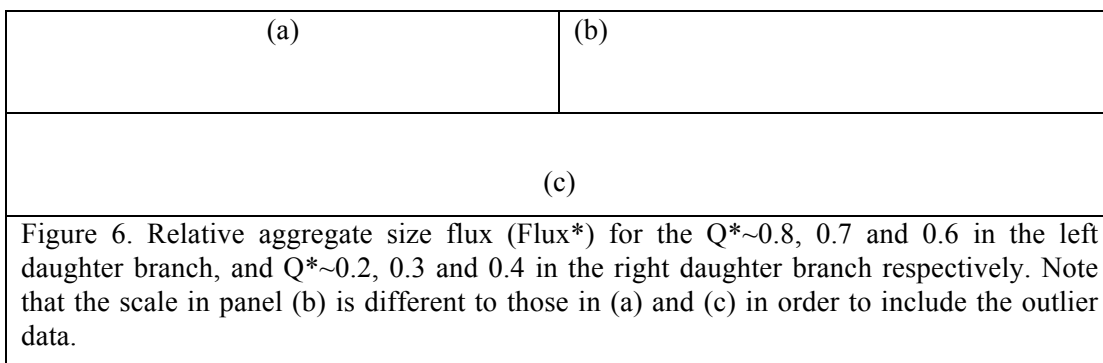
sizes  $A^*$  in the channel for a  $Q^* \sim 0.02$ .  $A^*$  values above 3 are shown and for 5 processed images for clarity of presentation. The channel height is not drawn to scale.

The existence of a distribution of aggregate sizes in the parent branch implies that these structures might be transported to the daughter branches at a variety of rates depending on the flow conditions in the geometry. Moreover, the findings regarding the reduction of mean aggregate size in the low  $Q^*$  branches [15] suggest that the transportation of aggregates of certain sizes might be affected. In order to examine the transportation characteristics of aggregates of different sizes, fluxes were calculated for aggregate sizes ( $A^*$ ) ranging from 1 to 7. The aggregate flux was examined initially for three different flow ratios giving  $Q^* \sim 0.2$ , 0.3 and 0.4 for the right daughter branch and  $\sim 0.8$ , 0.7, and 0.6 for the left daughter branch respectively. The results are presented in Figure 5.



As it can be seen from Figure 5 above, the flux of aggregates in the parent branch generally decreases with the increase of  $A^*$  for all flow split ( $Q^*$ ) cases and it is low for the larger aggregate sizes. This may be attributed to the fact that there is a smaller amount of large structures in the flow (see also the distribution in Figure 4a) compared to the smaller aggregates. In addition, it has been previously reported [15], and it is also observed in Figure 4b, that larger structures tend to concentrate in the centre of the flow, whereas smaller structures are more uniformly distributed, attaining high velocities also. As expected the  $A^*$  fluxes in the daughter branches are lower compared to these in the parent branch, however the differences diminish as  $A^*$  increases.

In order to examine the effect of the flow ratio ( $Q^*$ ) on aggregate fluxes, the relationship between fluxes in the parent and daughter branches was examined for the same aggregate sizes, using the normalised flux  $F^*$  quantity, for the left and right daughters respectively. This quantity is presented in Figure 6 below.



The results in Figure 6 illustrate an increasing trend of the relative aggregate flux  $F^*$  with increasing the aggregate size for the flow split ( $Q^*$ ) cases examined here. However, no clear dependency on  $Q^*$  value can be observed. This behaviour could be explained by considering the changes in the flow conditions and the structural characteristics in the daughter branches as  $Q^*$  is varied. Our earlier work illustrated that the concentration of cells becomes heterogeneous in the daughter branches as the flow ratio decreases resulting in skewed

velocity profiles [11,12]. A similar behaviour should be expected for the aggregates examined in the present study ( $Q^* \sim 0.8, 0.7$  and  $0.6$  and the opposite values) and reflected in the flux calculations.

A more complete picture on the influence of  $Q^*$  on  $F^*$  for the examined  $A^*$  values is provided in Figure 7. It is observed that the aggregate flux in the daughter branch is negligible for flow ratios below 0.5 and for the smaller  $A^*$  sizes. This can be attributed to the very low number of small structures, the low velocities and the reduced cell concentration, in these branches [12]. It is known that blood viscosity depends positively on aggregation and haematocrit and decreases with shear rate (shear thinning behaviour). Hence it can be postulated that the observed decrease in aggregate size and haematocrit in the low flow ratio branches counterbalance the decrease of the effective shear rate in these branches in order to prevent an increase in viscosity that could compromise flow [15].

In our previous work it was also shown that the cell and aggregate concentration is skewed towards one channel wall in the daughter branches [12]. The low velocities in the low  $Q^*$  branches would imply lower shear and less RBC migration to the channel centre. However, closer to the channel walls the shear stresses are higher and may contribute to suppressing further aggregate formation. On the other hand at the higher flow rates ( $Q^*$  greater than 0.5) the higher velocity gradients at the wall may promote RBC migration to the lower shear regions towards the channel centre, contributing to aggregate formation. Clear evidence of this axial migration, however, is not present in the flow fields produced (Figure 2). However, an increased mean  $A^*$  has been reported for  $Q^*$  values above  $\sim 0.2$  compared to the mean  $A^*$  in the parent branch [15]. Reasons for this  $A^*$  increase include the reduction of the shear forces in the daughter branches compared to the parent branch, the higher compactness and higher rate of interaction between cells and aggregates.

The shaded plane and the red lines in Figure 7 indicate an  $F^*$  value of one, i.e. the flux of the daughter branch is equal to the flux of the parent branch in these flow ratios. Data above this plane illustrate that aggregate fluxes in the daughter branches are higher than the ones in the parent branch. The relative fluxes with values greater than unity observed for  $A^*$  above 3, at the higher  $Q^*$ , imply that there is an efficient transport of these sizes in the bifurcating geometry studied here. In addition it is observed that the higher the aggregate size the greater the relative flux  $F^*$  for all flow ratios, which also implies lower resistance to transporting large aggregates in bifurcations.

<p>Figure 7: Normalized flux <math>F^*</math> (denoted here as Flux<math>^*</math>) of aggregate sizes (<math>A^*</math>) ranging from 1 to 7 at 34 split flow cases (i.e. 68 flow ratios <math>Q^*=0.0205-0.9562</math>). The shaded plane and the red lines indicate <math>F^*=1</math>, i.e. the conditions for which the flux of the daughter branch is equal to the flux of the parent branch.</p>
---

The fact that larger aggregates show higher relative fluxes, may also have a physiological significance, as it implies that the transport of the larger structures becomes more efficient downstream the bifurcations. This observation however, applies to bifurcating geometries of similar dimensions as in the current case, which nevertheless, are commonly encountered in the microcirculation [27]. It may help explain why RBC aggregation is not as deleterious for the human microcirculation as it is expected. Indeed, the evidence in the literature regarding the effect of RBC aggregation on vascular perfusion is not conclusive. Studies report non-monotonic increases of vascular resistance with RBC aggregation [28]; i.e. the vascular resistance decreases with aggregation before it increases again.

The present data suggest that the larger aggregates are efficiently transported downstream of a bifurcating flow configuration for a range of flow ratios, and preferentially flow through the high flow rate branch. This implies that the shearing forces required to disperse these

aggregates are not sufficiently high within these regions as discussed earlier. Viscosity data could not be acquired in the present experimental set up; however in one of our earlier studies [12], using a haematocrit-dependent viscosity model [29], it was shown that RBC aggregation caused a reduction on the local relative viscosity, in comparison to the non-aggregating cases. Although this viscosity information seems counterintuitive, as aggregation tends to increase the bulk viscosity of blood, it may suggest that the existence of large aggregates is not expected to heavily impact the flow. Further work is required to shed light on the aforementioned issues, including alterations of the aggregation intensity.

## **Conclusions**

RBC aggregation results in a distribution of aggregates in the microscale. Previous studies by the authors [11-15] using an idealised bifurcating microchannel geometry (T-junction) illustrated the effects of RBC aggregation on the structural and flow characteristics. In the present work additional structural characteristics regarding the flow of aggregates of specific sizes in the channel were analysed. The aggregate size distributions in the entire channel are exponential in nature, and agree qualitatively very well with those observed in previous studies [30].

Analysis of the aggregate transport through the bifurcating microchannel revealed that the flux of aggregates decreases with increasing aggregate size in both the parent and the daughter branches in absolute terms. However, the flux relatively to the parent branch,  $F^*$ , increases in the daughter branch, for large aggregates ( $A^*$  above  $\sim 3$ ) and for high flow ratios  $Q^*$ . This intriguing behaviour is explained on the basis of the structural (cell/aggregate concentration) and flow characteristics in the channel (flow rate differences in the branches, flow split location) and could provide some clues on the non-destructive nature of RBC aggregation in physiological blood flow, which remains a subject of controversy: the increase of the relative flux  $F^*$  in the higher flow daughter branches, in conjunction with the reduced relative viscosity observed in earlier studies therein [13], imply no significant adverse effects of aggregates on the flow of blood in that scale.

The work may also provide valuable information regarding biomicrofluidic applications. As whole blood manipulation in microfluidic devices is required in many applications, detailed knowledge of the structural and flow characteristics could aid towards a more efficient design of such devices.

## **Acknowledgements**

The authors would like to thank Dr. Peter Vennemann for providing the free PIV analysis software JPIV ([www.jpiv.vennemann-online.de](http://www.jpiv.vennemann-online.de)).

## **Conflict of interest statement**

No conflict of interest to declare.

## **Funding**

The study has been supported with funding from the internal Start-up Grants of the Cyprus University of Technology.

## **Ethical Approval**

The study has been approved by the Southeast London Ethics Committee (ref: 10/H0804/21).

## References.

- [1] Mehri R, Laplante J, Mavriplis C, Fenech M. Investigation of blood flow analysis and red blood cell aggregation. *J.Med.Biol.Eng.* 2014;34(5):469-74.
- [2] Yeom E, Lee SJ. Microfluidic-based speckle analysis for sensitive measurement of erythrocyte aggregation: A comparison of four methods for detection of elevated erythrocyte aggregation in diabetic rat blood. *Biomicrofluidics* 2015;9(2):024110.
- [3] Meiselman HJ, Neu B, Rampling MW, Baskurt OK. RBC aggregation: Laboratory data and models. *Indian.J.Exp.Biol.* 2007;45(1):9-17.
- [4] Copley AL, King RG, Chien S, Usami S, Skalak R, Huang CR. Microscopic observations of viscoelasticity of human blood in steady and oscillatory shear. *Biorheology* 1975;12(5):257-63.
- [5] Thurston GB. Elastic effects in pulsatile blood flow. *Microvasc.Res.* 1975;9(2):145-57.
- [6] Thurston GB. The viscosity and viscoelasticity of blood in small diameter tubes. *Microvasc.Res.* 1976;11(2):133-46.
- [7] Tomaiuolo G, Carciati A, Caserta S, Guido S. Blood linear viscoelasticity by small amplitude oscillatory flow. *Rheol.Acta* 2016;55(6):485-95.
- [8] Sousa PC, Pinho FT, Alves MA, Oliveira MSN. A review of hemorheology: Measuring techniques and recent advances. *Korea Aust.Rheol.J.* 2016;28(1):1-22.
- [9] Tomaiuolo G, Lanotte L, Ghigliotti G, Misbah C, Guido S. Red blood cell clustering in Poiseuille microcapillary flow. *Phys.Fluids* 2012;24(5).
- [10] Clavería V, Aouane O, Thiébaud M, Abkarian M, Coupier G, Misbah C, et al. Clusters of red blood cells in microcapillary flow: Hydrodynamic: versus macromolecule induced interaction. *Soft Matter* 2016;12(39):8235-45.
- [11] Sherwood JM, Dusing J, Kaliviotis E, Balabani S. The effect of red blood cell aggregation on velocity and cell-depleted layer characteristics of blood in a bifurcating microchannel. *Biomicrofluidics* 2012;6(2):024119.
- [12] Sherwood JM, Kaliviotis E, Dusing J, Balabani S. Hematocrit, viscosity and velocity distributions of aggregating and non-aggregating blood in a bifurcating microchannel. *Biomech.Model.Mechanobiology* 2014;13(2):259-73.
- [13] Sherwood JM, Holmes D, Kaliviotis E, Balabani S. Spatial distributions of red blood cells significantly alter local haemodynamics. *PLoS ONE* 2014;9(6):e100473.
- [14] Kaliviotis E, Dusing J, Sherwood JM, Balabani S. Quantifying local characteristics of velocity, aggregation and hematocrit of human erythrocytes in a microchannel flow. *Clin.Hemorheol.Microcirc.* 2016;63(2):123-48.
- [15] Kaliviotis E, Sherwood JM, Balabani S. Partitioning of red blood cell aggregates in bifurcating microscale flows. *Scientific Reports* 2017;7, DOI: 10.1038/srep44563.

- [16] Kaliviotis E. Mechanics of the red blood cell network. *Journal of Cellular Biotechnology* 2015;1:37-43.
- [17] Baskurt OK, Uyuklu M, Ulker P, Cengiz M, Nemeth N, Alexy T, et al. Comparison of three instruments for measuring red blood cell aggregation. *Clin.Hemorheol.Microcirc.* 2009;43(4):283-98.
- [18] Baskurt OK. In vivo correlates of altered blood rheology. *Biorheology* 2008;45(6):629-38.
- [19] Chien S, Jan K-. Ultrastructural basis of the mechanism of rouleaux formation. *Microvasc.Res.* 1973;5(2):155-66.
- [20] Flormann D, Schirra K, Podgorski T, Wagner C. On the rheology of red blood cell suspensions with different amounts of dextran: separating the effect of aggregation and increase in viscosity of the suspending phase. *Rheol.Acta* 2016;55(6):477-83.
- [21] Lipowsky HH, Usami S, Chien S. In vivo measurements of "apparent viscosity" and microvessel hematocrit in the mesentery of the cat. *Microvasc.Res.* 1980;19(3):297-319.
- [22] Lipowsky HH. Microvascular rheology and hemodynamics. *Microcirculation* 2005;12(1):5-15.
- [23] Koutsiaris AG, Tachmitzi SV, Batis N, Kotoula MG, Karabatsas CH, Tsironi E, et al. Volume flow and wall shear stress quantification in the human conjunctival capillaries and post-capillary venules in vivo. *Biorheology* 2007;44(5-6):375-86.
- [24] Koutsiaris AG. Hemodynamics in the Microcirculation. *Ann.Biomed.Eng.* 2016;44(4):1321-2.
- [25] Kaliviotis E, Ivanov I, Antonova N, Yianneskis M. Erythrocyte aggregation at non-steady flow conditions: A comparison of characteristics measured with electrorheology and image analysis. *Clin.Hemorheol.Microcirc.* 2010;44(1):43-54.
- [26] Guidi L, Jackson GA, Stemmann L, Miquel JC, Picheral M, Gorsky G. Relationship between particle size distribution and flux in the mesopelagic zone. *Deep-Sea Res.Part I Oceanogr.Res.Pap.* 2008;55(10):1364-74.
- [27] Frame MDS, Sarelius IH. Arteriolar bifurcation angles vary with position and when flow is changed. *Microvasc.Res.* 1993;46(2):190-205.
- [28] Yalcin O, Uyuklu M, Armstrong JK, Meiselman HJ, Baskurt OK. Graded alterations of RBC aggregation influence in vivo blood flow resistance. *Am.J.Physiol.Heart Circ.Physiol.* 2004;287(6 56-6):H2644-50.
- [29] Pries AR, Neuhaus D, Gaehtgens P. Blood viscosity in tube flow: Dependence on diameter and hematocrit. *Am.J.Physiol.Heart Circ.Physiol.* 1992;263(6 32-6):H1770-8.
- [30] Karabetsos E, Papaodysseus C, Koutsouris D. Design and development of a new ultrasonic doppler technique for estimation of the aggregation of red blood cells. *Meas J Int Meas Confed* 1998;24(4):207-15.



Figure 1

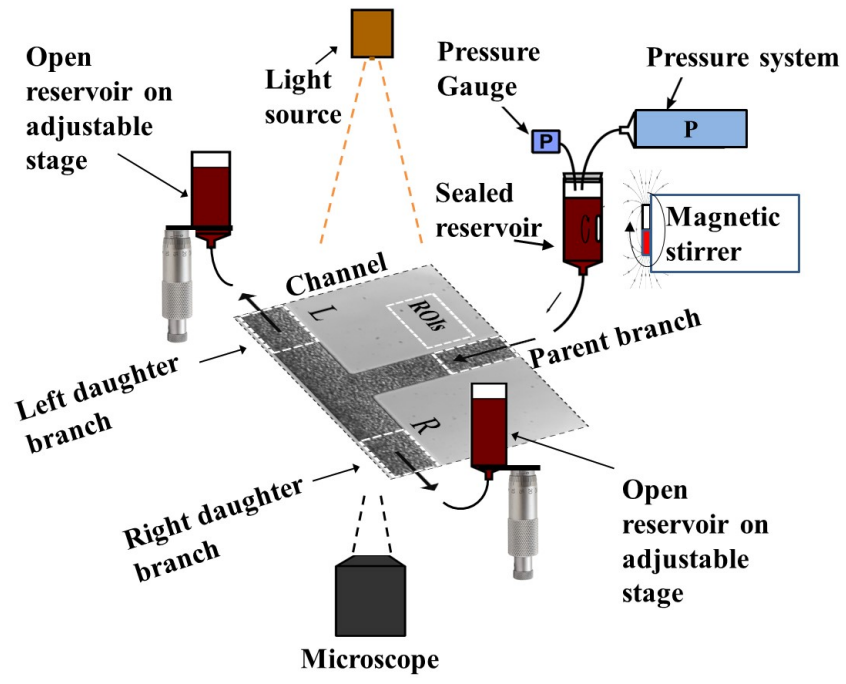


Figure 1.

Figure 2

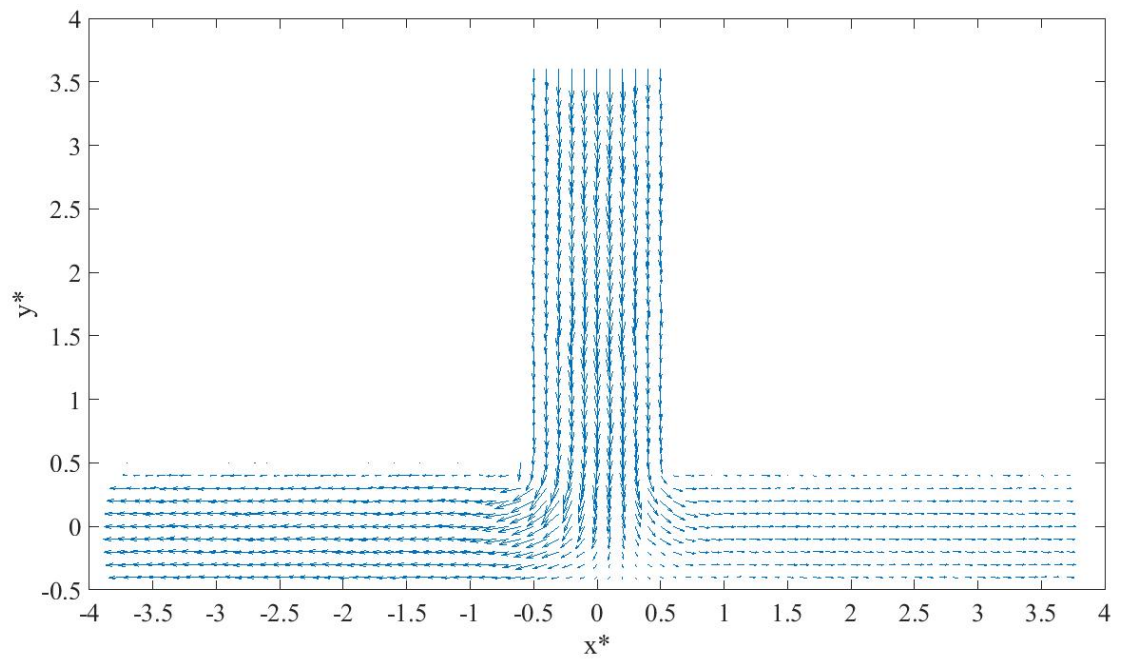


Figure 2

Figure 3

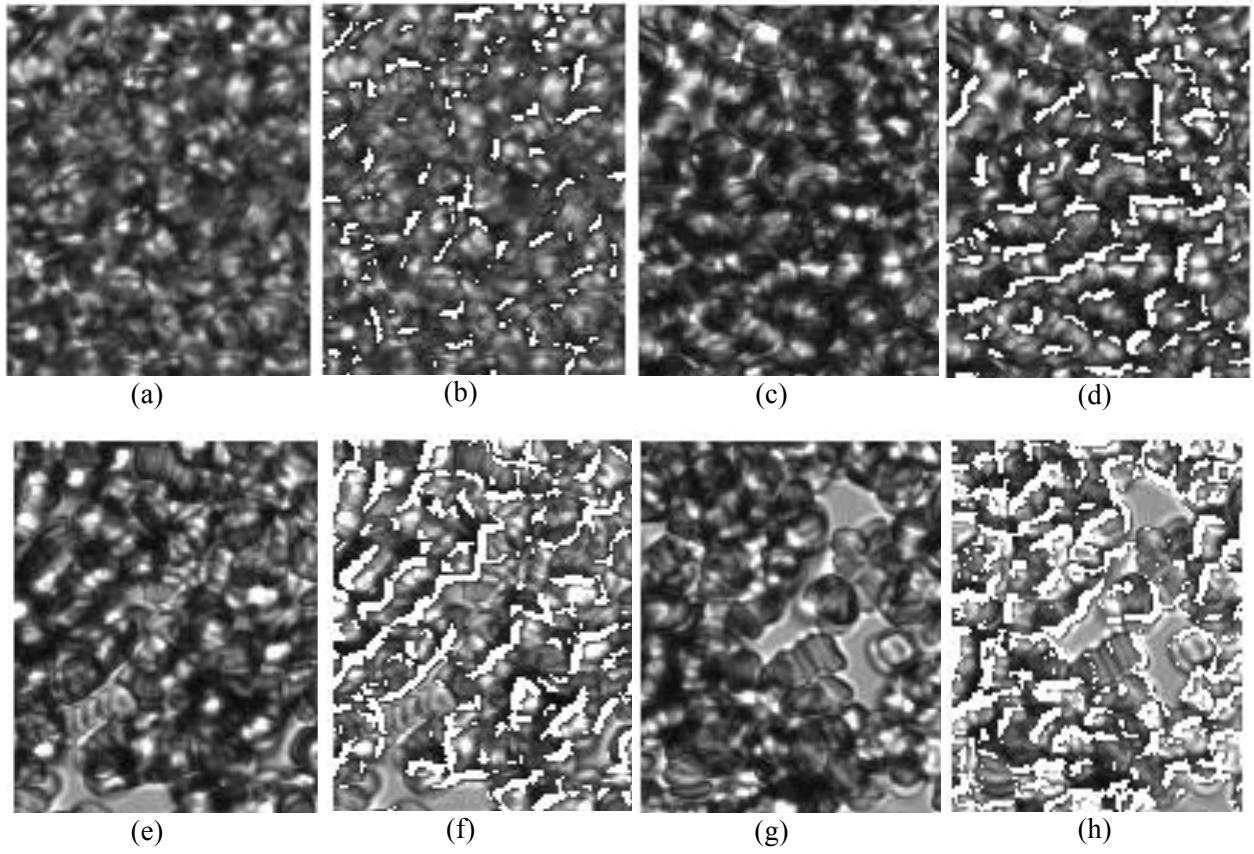


Figure 3.

Figure 4

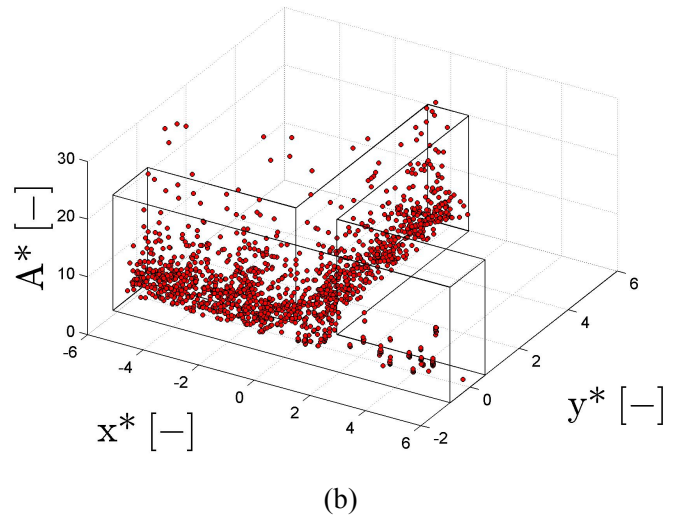
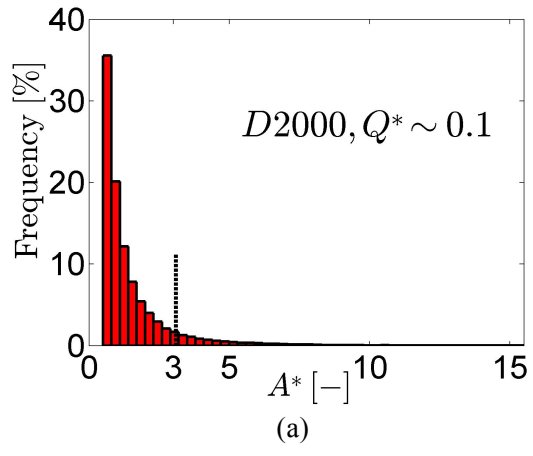
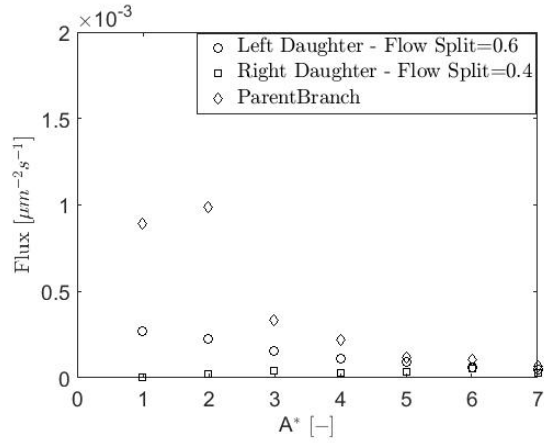
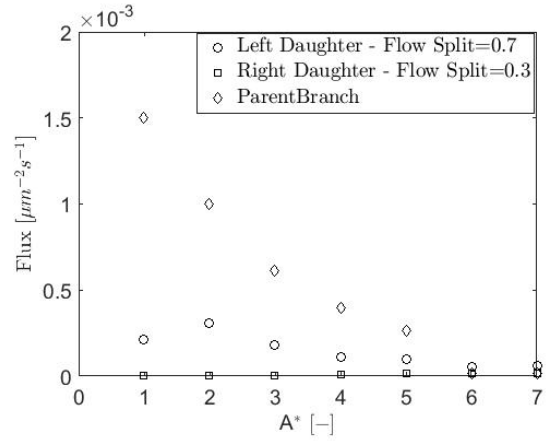


Figure 4

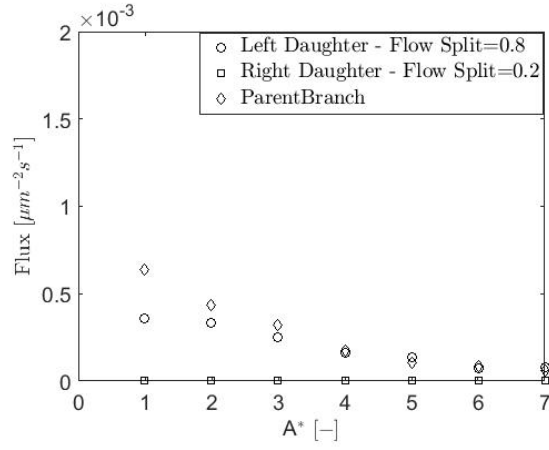
Figure 5



(a)



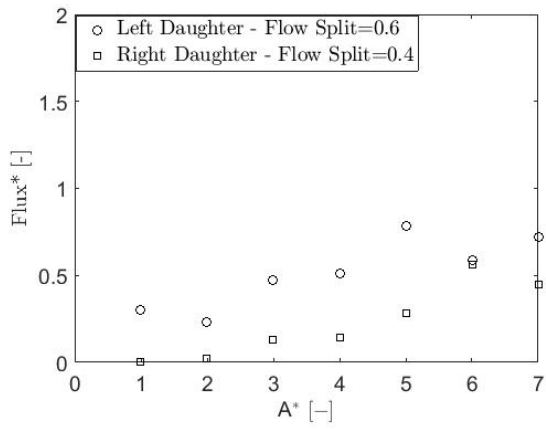
(b)



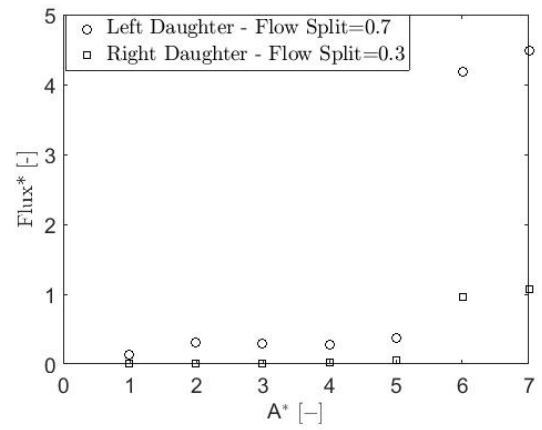
(c)

Figure 5.

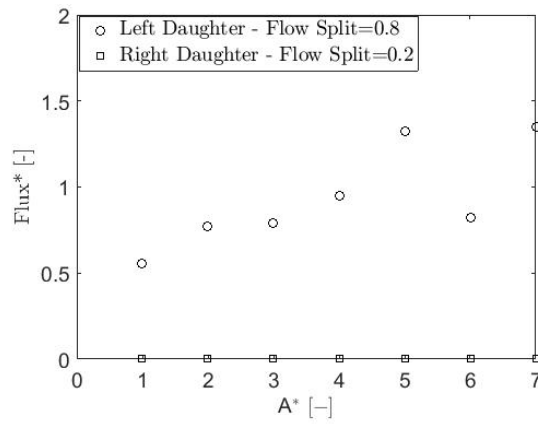
Figure 6



(a)



(b)



(c)

Figure 6.

Figure 7

